IGWs and WDs Ongoing Writeup

Yubo Su

I. INTRODUCTION

WIP ongoing writeup, last updated December 6, 2018.

Basic narrative is: the prevailing understanding is that mean flow absorption slowly spins up a WD from the outside in as the critical layer propagates inwards. Our numerical simulations validate this prediction and give an analytical prediction for the motion of the critical layer. However, it appears our numerical simulations are viscosity limited. We present a brief argument for why the viscosity limitations are insignificant, but also present some exploratory, inconclusive work towards direct numerical simulation resolving critical layer behavior without being viscosity limited.

In §II, we will cover the equations and numerical setup. In §III, we will discuss the agreement of our simulation in the low-amplitude limit with analytical linear theory. In §IV we will present a few reference simulations illustrating critical layer absorption depositing horizontal angular momentum into the fluid. Finally, in §V we will consider a speculative series of simulations attempting to rectify the seemingly viscosity-limited simulations of the previous section.

II. EQUATIONS

We simulate an incompressible, isothermal fluid, representatitive of degenerate matter in WD bulks. We assume a barotropic equation of state as a first approximation. Furthermore, we model the background, hydrostatic density stratification as $\rho_0(x,z) = \rho_0(z) \propto e^{-z/H}$.

The physical equations for an incompressible, barotropic fluid in a uniform gravitational field are

$$\vec{\nabla}\cdot\vec{u} = 0, \tag{1a}$$

$$\frac{\partial\rho}{\partial t} + \vec{u}\cdot\vec{\nabla}\rho = 0, \tag{1b}$$

$$\frac{\partial\vec{u}}{\partial t} + \left(\vec{u}\cdot\vec{\nabla}\right)\vec{u} + \frac{\vec{\nabla}P}{\rho} + g\hat{z} = 0. \tag{1c}$$

$\vec{u}, \rho, P$ are the fluid dynamical variables and $-g\hat{z}$ is constant gravitational acceleration. Note that at hydrostatic equilibrium $\partial_t = 0$ we have $\vec{u} = 0, \vec{\nabla}P_0 = -\rho_0 g\hat{z}$ and so $P_0 = \rho_0 g H$.

We nondimensionalize by taking $H = N = \rho_{ref} = 1$ where

$$N^2 \equiv g^2\left(\frac{\mathrm{d}\rho}{\mathrm{d}P} - \left.\frac{\partial\rho}{\partial P}\right|_{ad}\right) = \frac{g}{H}, \tag{2}$$

is the Brunt-Väisälä frequency and ρ_{ref} is the background density stratification at $z = 0$. The full numerical details of the simulation are described in §A 1.

A. Wave Generation

To model a continuous IGW wave train excited deep in the WD interior propagating towards the surface without unnecessary computational cost, we excite an IGW wave train from the bottom of the simulation domain. As Chebyshev grid is a factor of $\propto N_z$ denser near the edges of the simulation domain, we use a volumetric forcing to excite IGW at some $z_0 > 0$ interior to the simulation domain. Our forcing excites both IGW propagating upwards, the physically interesting solution, and downwards, which are damped away by damping layers (see §A 1) before inducing strict Courant-Friedrichs-Lewy (CFL) timestepping constraints (cite).

As not to interfere with the incompressibility constraint, we force the system on the density equation, replacing Eq. 1b with

$$\frac{\partial\rho}{\partial t} + \vec{u}\cdot\vec{\nabla}\rho = Fe^{-\frac{(z-z_0)^2}{2\sigma^2}}\cos(k_{0,x}x - \omega_0 t). \tag{3}$$

Define $k_{0,z} : \omega(k_{0,x}, k_{0,z}) = \omega_0$. If $k_{0,z}\sigma \ll 1$, the forcing term has the effect of picking out $k_{0,z}$ driven by $\cos(k_{0,x}x - \omega_0 t)$ from the broad k_z wavenumber spectrum permitted by the narrow Gaussian profile.

III. LINEAR REGIME

We first test our numerical simulation with a "linear" simulation, where all flow quantities are small: we assume $\rho_1 \equiv \rho - \rho_0 \ll \rho_0$ and $\vec{u}\cdot\vec{\nabla} \ll \partial_t$. We clarify that our "linear" simulations solve the full nonlinear equations, just in the weak perturbation limit.

A. Analytical Solution

In the small perturbation limit, we linearize Eq. 1 with inhomegeneous driving term and obtain:

$$\vec{\nabla}\cdot\vec{u}_1 = 0, \tag{4a}$$

$$\frac{\partial\vec{u}_1}{\partial t} + \frac{\vec{\nabla}P}{\rho_0} + \frac{\rho_1\vec{g}}{\rho_0} = 0, \tag{4b}$$

$$\frac{\partial\rho_1}{\partial t} - \frac{u_{1z}\rho_0}{H} = Fe^{-\frac{(z-z_0)^2}{2\sigma^2}}e^{i(k_x x - \omega t)}. \tag{4c}$$

We have substituted $\cos(k_x x - \omega_0 t)$ for a complex exponential for easier manipulation; taking real parts of all dynamical variables above recovers the physical solution.

It is well known that the solutions to the $F = 0$ homogeneous Eq. 4 are of form (cite)

$$u_z(x,z,t) = Ae^{z/2H} e^{i(k_{0x}x + k_{0z}z - \omega_0 t)}, \tag{5a}$$

$$\omega_0^2 = \frac{N^2 k_{0x}^2}{k_{0x}^2 + k_{0z}^2 + \frac{1}{4H^2}}. \tag{5b}$$

To solve the inhomogeneous system, we may first approximate the driving term using $e^{\frac{-(z-z_0)^2}{2\sigma^2}} \approx \sqrt{2\pi\sigma^2}\delta(z - z_0)$ if $\sigma \to 0$, then relax to $k_{0z}\sigma \lesssim 1$. This may be solved to obtain the solution

$$A(F) = \frac{Fgk_{0x}^2}{\rho_0(z_0)\omega_0^2} \frac{1}{2ik_z} \frac{e^{\frac{-(k_{0z}\sigma)^2}{2}}}{\sqrt{2\pi\sigma^2}}, \tag{6}$$

$$u_{1z} = A(F) \times \begin{cases} e^{\frac{z-z_0}{2H}} e^{i(k_{0x}x + k_{0z}(z-z_0) - \omega_0 t)} & z > z_0 \\ e^{\frac{z-z_0}{2H}} e^{i(k_{0x}x - k_{0z}(z-z_0) - \omega_0 t)} & z < z_0 \end{cases}. \tag{7}$$

The extra factor of $e^{-\frac{(k_{0z}\sigma)^2}{2}}$ compared to the δ-function solution comes from evaluating the Fourier Transform of $e^{-\frac{(z-z_0)^2}{2\sigma^2}}$ at $k_z = k_{0z}$.

Furthermore, in the low-amplitude, dissipation free limit, the time-averaged total x-momentum flux in the $\hat{z}$ direction can be computed. Since all dynamical variables $\propto e^{i(k_{0x}x - \omega_0 t)}$, x averaging and time averaging are equivalent, so we may write

$$F_{px} \equiv \frac{1}{L_x} \int_0^{L_x} \rho u_x u_z \, \mathrm{d}x \tag{8}$$

We will denote this $F_{px} = \langle \rho u_x u_z \rangle_x$ for simplicity. For a given forcing amplitude then:

$$F_{px}(F) \approx -\frac{A(F)^2}{2} \rho_0(z_0) \frac{k_z}{k_x}. \tag{9}$$

We've approximated $k_z H \ll 1$ and noticed $\langle \rho_1 u_x u_z \rangle_x = 0$ in the above for clarity.

Finally, it may be noted that horizontally averaged horizontal momentum $p_x = \langle \rho u_x \rangle_x$ obeys $\frac{\partial p_x}{\partial t} + \frac{\partial F_{px}}{\partial z} = 0$, and since flux is transported on the group velocity timescale, this simplifies to the known expression for the wave-induced horizontal mean flow (cite)

$$\bar{U}_0 \equiv \langle u_x \rangle_x = \frac{\langle u_x u_z \rangle_x}{c_{gz}} \tag{10}$$

We've denoted $c_{gz} = \frac{\partial \omega}{\partial k_z}\Big|_{k_{z0}}$ the vertical group velocity. In terms of our forcing amplitude,

$$\bar{U}_0(F) = -\frac{A(F)^2}{2} e^{\frac{z-z_0}{H}} \frac{k_z}{k_x} c_{gz}, \tag{11}$$

where $c_{gz} = -\frac{N k_{0x} k_{0z}}{\left(k_{0x}^2 + k_{0z}^2 + \frac{1}{4H^2}\right)^{3/2}}$.

ω is chosen by inverting $\omega(k_x, k_z)$ dispersion relation for fixed $k_x = 2\pi/L_x$ and some desired $k_z = -2\pi/H$, and $\sigma \lesssim \frac{1}{k_z}$ is used to excite a broad band of modes including the desired k_z mode.

B. Numerical Simulation

We simulate using Dedalus (cite) a spectral numerical method. We use a Fourier basis in the x direction and a Chebyshev in the z direction. Our simulation starts with all perturbation quantities at zero, an initial condition at rest. Our parameters are chosen to be as similar as possible to the later nonlinear simulations (§IV). We choose as follows:

- k_{0x}: Astrophysical IGWs have $k_x \ll k_z$, so we choose $k_{0x} = \frac{2\pi}{L_x}$ the smallest permitted wavenumber permitted by periodic boundary conditions.

- We choose ω_0 by choosing it to produce a desired k_{0z}. Astrophysical systems generally also exhibit $k_z H \gg 1$, where the stratification height is significantly larger than the vertical wavelength. However, in order for the simulation to both be well-damped at grid resolutions and be neglibily damped at leading order nonlinear wavelengths, we require $k_{0z} \ll \frac{1}{L_{NL}} \ll \frac{2\pi N_z}{L_z}$, where L_{NL} denotes some characteristic length scale of nonlinear features. Finally, we need L_z to be many H to capture significant $e^{z/2H}$ growth and separate the linear and nonlinear amplitudes of u_z.

  Fixing $L_z = 10H$ to give $\sim e^4$ amplitude growth between the damping zones, this implies we require separation of scales $1 \ll k_{0z}H \ll \frac{H}{L_{NL}} \ll \frac{2\pi N_z}{10}$.

  Since N_z is fixed by computational cost (we tried both $N_z = 512, N_z = 1024$), we choose $k_{0z} \sim \frac{2\pi}{H}$. This is less physically representative but gives more wavenumber space for the nonlinear cascade. We then invert $\omega_0 = \omega(k_{0x}, k_{0z})$.

- We choose ν 1/10 that of the nonlinear simulation, to verify that the undamped linear solution is recovered.

- We choose F forcing strength 1/20 that of the nonlinear simulation, which keeps the flow amplitude sufficiently small to be treated in the linear approximation at all points in the simulation domain.

A representative snapshot of this simulation is provided in Fig. 1. Key features to note:

- u_z grows with Eq. 7 to reasonable accuracy.
- F_{px} is seen to be constant, as would be expected by Eq. 9.
- $\bar{U}_0$ agrees with Eq. 11 at lower z but deviates significantly at higher z. This deviation is caused by the top damping zone that does not conserve horizontal momentum.

We also include a qualitatively similar snapshot of the same simulation run using the ν from the later nonlinear simulations in Fig. 2.

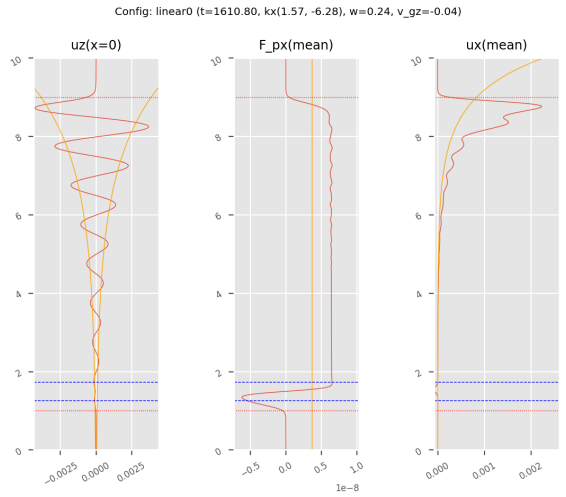

FIG. 1: Snapshot of linear simulation after reaching steady state. Analytical predictions of $|u_z|, \bar{U}_0, F_{px}$ are shown in orange. Red dotted lines indicate the onset of the damping region and blue dotted lines denote the driving region.

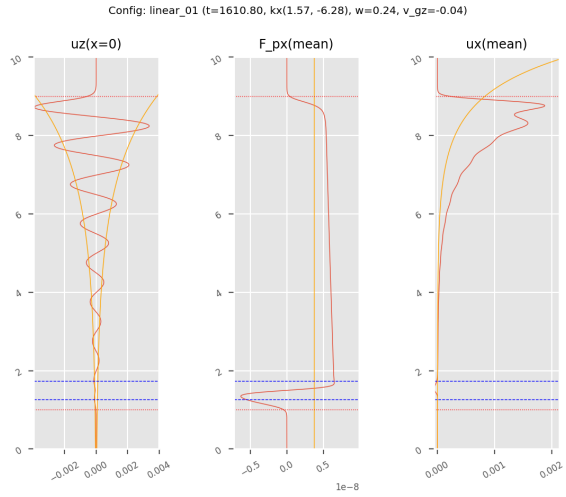

FIG. 2: Same as Fig. 1 but with 0.3×viscosity used for nonlinear simulations (YUBONOTE should be the same but that simulation mysteriously stopped without me noticing; restarting worked, so currently rerunning). Note the slight resulting dissipation in F_{px}.

IV. NONLINEAR REGIME

A. Mean Flow Critical Layer Absorption

In past studies of IGWs in WDs (cite Fuller & Lai), $\xi_z \equiv \frac{u_z}{\omega_0}$ the Lagrangian fluid displacement was often used towards wave breaking criterion $k_{0z}\xi_z \gtrsim 1$. We argue that the wave's self-interaction via its generated mean flow $\bar{U}_0$ induces total absorption when the mean flow exceeds critical value

$$\bar{U}_c = \frac{\omega_0}{k_{0x}}. \tag{12}$$

This is consistent with the picture put forth in e.g. Goldreich and Nicholson (cite).

A purely horizontal shear flow $\bar{U}_0(z)\hat{x}$ can be seen in Eq. 1 to have the effect of modifying time derivatives ∂_t to their frequency in the comoving frame of the fluid $\partial_t - \bar{U}_0(z)\partial_x$. For a critical value $\omega_0 - \bar{U}_c k_{0x} = 0$, the frequency of the linear wave in the fluid's frame of reference vanishes and critical behavior is observed. In a linear theory or a theory where small scales are viscosity rather than advection dominated, the incident wave has amplitude reflection and transmission coefficients

$$\mathcal{R} = e^{-2\pi\sqrt{\mathrm{Ri}-\frac{1}{4}}}, \qquad \mathcal{T} = e^{-\pi\sqrt{\mathrm{Ri}-\frac{1}{4}}}, \tag{13}$$

where we have defined Richardson number $\mathrm{Ri} \equiv \left.\frac{N^2}{\left(\frac{\partial \bar{U}_0}{\partial z}\right)^2}\right|_{z_c}$ at the critical layer $z_c : \bar{U}_0(z_c) = \frac{\omega_0}{k_{0x}}$. For most shear flows, $\mathrm{Ri} \gg 1$ and so $\mathcal{R}, \mathcal{T} \ll 1$ and the incident wave is absorbed.

When the fluid absorbs the incident wave, it absorbs the incident horizontal momentum flux as well, which is converted into additional horizontal momentum of the shear flow. Since the shear flow cannot exceed $\bar{U}_c$ the horizontal phase velocity of the incident wave, the critical layer must thus propagate downwards (towards the wave source) to accommodate the incident momentum. In other words, the total horizontal momentum of the shear flow obeys conservation equation

$$\frac{\partial}{\partial t}\int_0^{L_z} \rho(z)\bar{U}_0(z,t)\,\mathrm{d}z - F_{px} = 0. \tag{14}$$

Treating $\bar{U}_0(z > z_c) = \bar{U}_c, \bar{U}(z < z_c) = 0$ gives us exactly

$$\rho\bar{U}_c\frac{\partial z_c}{\partial t} = -F_{px}. \tag{15}$$

B. Numerical Simulation

We use the same k_{0x}, ω_0 as §III B. Our other parameters are:

- We choose $\nu = 0.35\frac{\omega_0}{k_{0z}k_{z,\max}}$, where $k_{z,\max} = \frac{2\pi N_z}{L_z}$.

Note that $\nu = \frac{\omega_0}{k_{0z} k_{z,\max}}$ corresponds to the advective term $\vec{u} \cdot \vec{\nabla}$ being of the same order as the time derivative ∂_t for flow velocities $\vec{u} \sim \frac{\omega_0}{k_{0z}}$ at the grid spacing.

- We choose F such that $\bar{U}_0(z)$ predicted by Eq. 11 exceeds $\bar{U}_c$ critical velocity for $z < L_z$, i.e. the wave-induced mean flow is sufficiently large within the simulation domain to induce critical layer absorption.

Two representative snapshots from our simulation are provided in Fig. 3 after the critical layer has had time to form. We may note that the critical layer, where F_{px} is absorbed and $\bar{U}_0 = \bar{U}_c$, travels downwards as predicted.

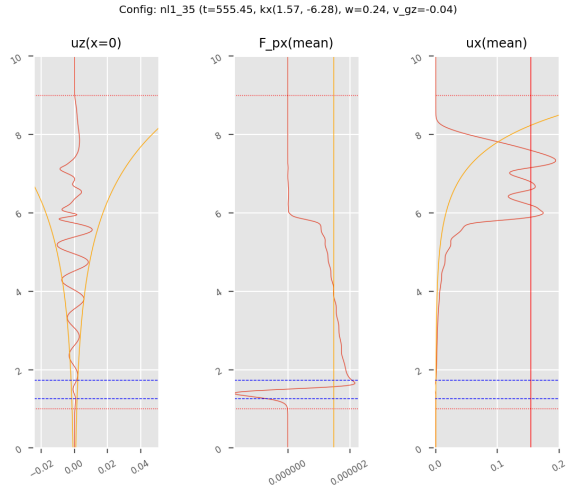

(a) Earlier time snapshot. Legend is the same as Fig. 1 except $\bar{U}_c$ is marked in red on the third panel.

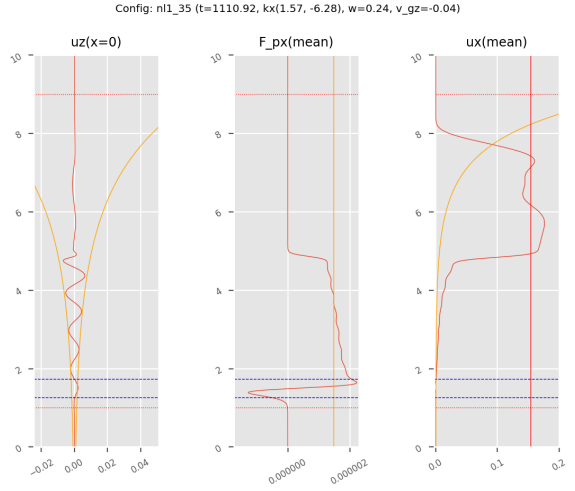

(b) Later snapshot illustrating propagation of z_c.

FIG. 3: Nonlinear numerical simulation.

C. Propagating Critical Layer

For the simulation in Fig. 3, we may define $z_c = \text{argmax}_z \frac{\partial \bar{U}_0}{\partial z}$. Computing $\frac{\partial z_c}{\partial t}$ using the analytical flux Eq. 9 allows comparison to Eq. 15, which we exhibit in Fig. 4. We see overall good agreement, though some small deviation is expected since F_{px} is not perfectly conserved owing to numerical viscosity (and YUBONOTE F_{px} is misestimated?).

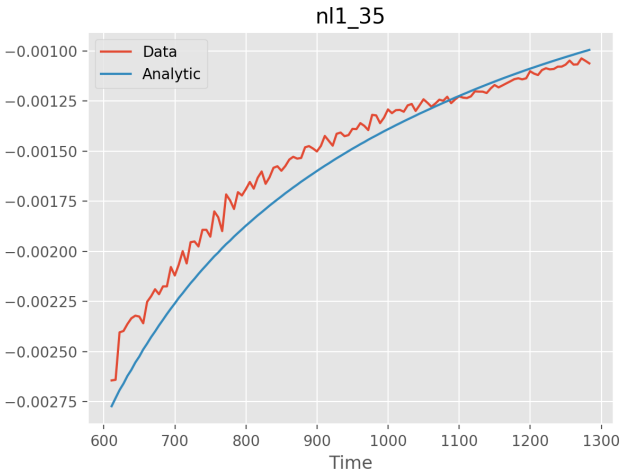

FIG. 4: Comparison of simulated $\frac{\partial z_c}{\partial t}$ to analytical Eq. 15. Plot begins after formation of critical layer in simulation.

However, recalling Eq. 13, we only expect complete critical layer absorption when $\text{Ri} \gg \frac{1}{4}$. We may plot Ri over the same time interval in Fig. 5. We may observe that the Richardson number is initially decreasing but eventually levels out and begins to increase again. This corresponds to an increasingly sharp critical layer transition then subsequently a decreasingly sharp critical layer transition.

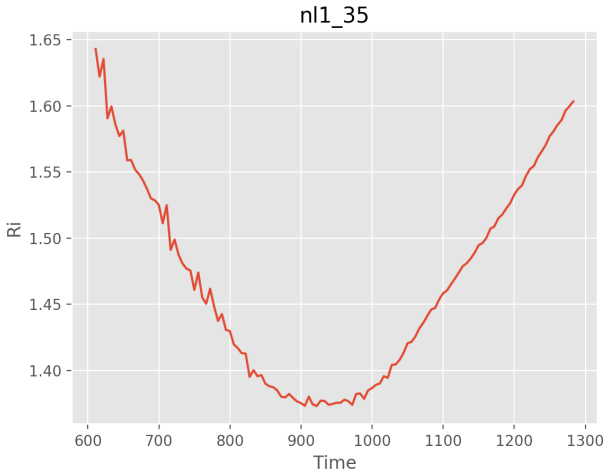

FIG. 5: Plot of $\text{Ri}_{\max}(t) = \max_z \frac{N^2}{\bar{U}_0'}(t)$ over the simulation time.

We argue that the Richardson number is bounded from below by viscosity. A repeated simulation with a larger viscosity is shown in Fig. 6, where the Richardson number does not go nearly as low.

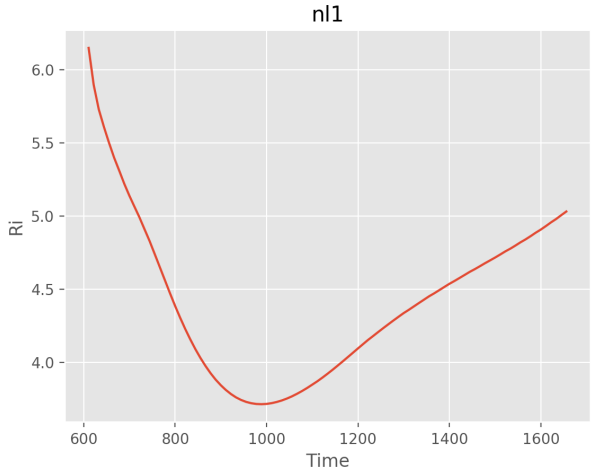

FIG. 6: Same as Fig. 5 but with $\sim 1.3\times$ viscosity.

Additionally, a lower-viscosity simulation shows significant features resembling Kelvin-Helmholtz instabilities (KHI), Fig. 7. As we have only plotted $\bar{U}_0(z)$, the local Richardson number $N^2/\frac{\partial u_x}{\partial z}$ may exceed the plotted value and incur KHIs.

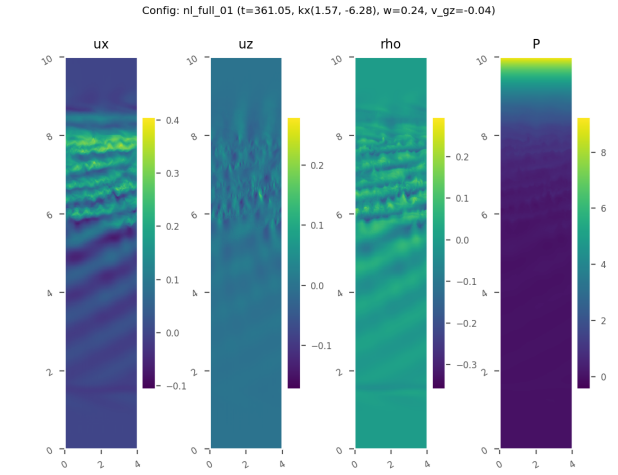

FIG. 7: Low viscosity simulation showing seemingly KHI-like features.

This seems to suggest that our reference simulation is viscosity limited. This is perhaps physical: a Richardson number ~ 0.25 incurs the KHI which saps energy and angular momentum from the flow. It is conceivable then that our numerical viscosity is physically motivated as a effective KHI viscosity.

V. BOUSSINESQ LOCAL SIMULATION (SPECULATIVE)

Alternatively, we can attempt direct numerical simulation probing lower Richardson numbers. We will move to the Boussinesq approximation and set up a mean flow as an initial condition. This relaxes the constraint that the domain must be sufficiently large to permit substantial $e^{z/H}$ growth of the mean flow $\bar{U}_0$ and allows us to probe much finer vertical resolution.

The physical equations in the Boussinesq approximation are:

$$\vec{\nabla}\cdot\vec{u} = 0, \tag{16a}$$

$$\frac{\partial \rho_1}{\partial t} + \left(\vec{u}\cdot\vec{\nabla}\right)\rho_1 - N^2\frac{\rho_0 u_z}{g} = 0, \tag{16b}$$

$$\frac{\partial \vec{u}}{\partial t} + \left(\vec{u}\cdot\vec{\nabla}\right)\vec{u} + \frac{\vec{\nabla}P_1}{\rho_0} + \frac{\rho_1 g\hat{z}}{\rho_0} = 0. \tag{16c}$$

In these equations, we take $\rho_0(z) = \rho_0 = 1$ a constant reference density. We nondimensionalize $\rho_0 = N = g = 1$. By using a subgrid model (details §A 2), we are able to probe significantly smaller Richardson numbers.

A. Low-Resolution Simulation

The parameters of the simulation differ slightly; since we do not have exponential density stratification to induce $\bar{U}_0 \propto e^{z/H}$ growth, we initialize the system with an initial $\bar{U}_0(z) \leq \bar{U}_c$, simulating a later phase of the stratified simulation where the critical layer has propagated deep into the domain.

Sample snapshots from a reference simulation are Fig. 8. The resulting front velocity and Richardson number are depicted in Fig. 9. Most important to note are the significantly diminished critical layer velocity compared to the prediction (owing to critical layer reflection) and the Richardson number which approaches the critical $1/4$ value for KHI-instability.

YUBONOTE: The next step would be to run simulations at sufficient resolution to resolve the KHI (only possible in the Boussinesq system, where we are not required to have a sufficiently large vertical domain to capture exponential growth and can choose ever smaller vertical domains); I have started to try this but haven't resolved the resultant numerical issues yet.

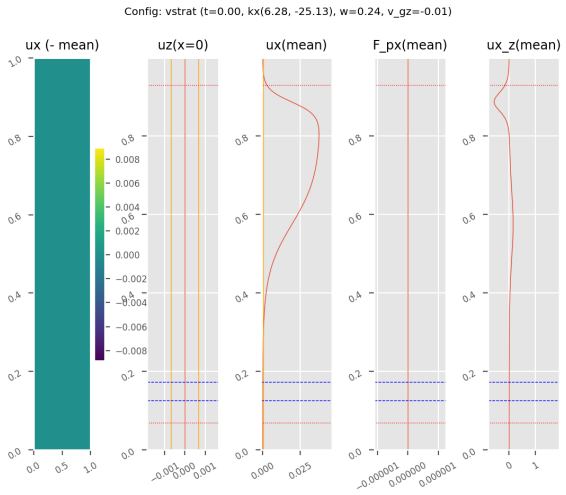

(a) Boussinesq simulation initial condition.

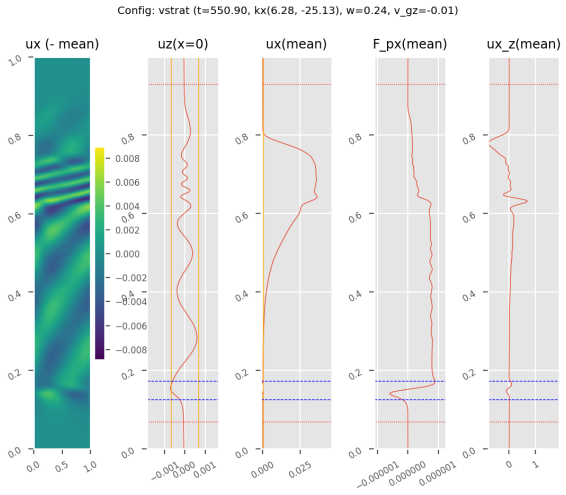

(b) At later time, when critical layer absorption has begun.

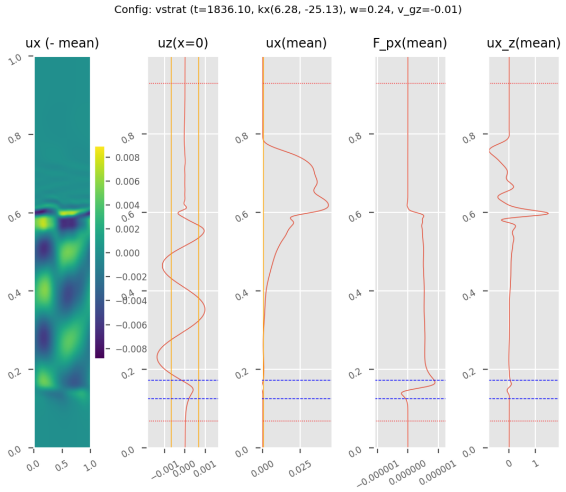

(c) At an even later time, a strong reflective character seems to emerge as the Richardson number $\to 0.5$.

FIG. 8: Boussinesq simulation snapshots.

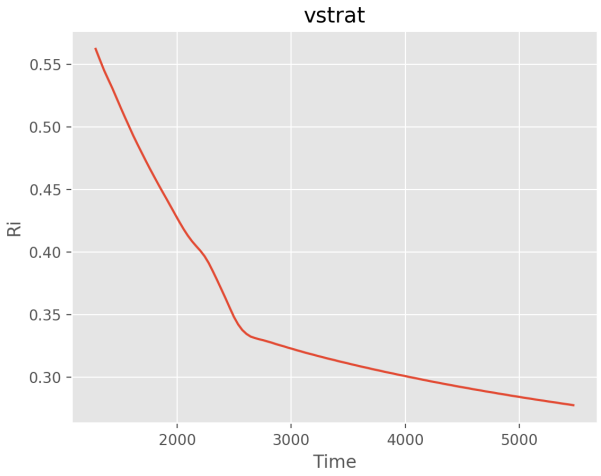

(a) Richardson number evolution over time.

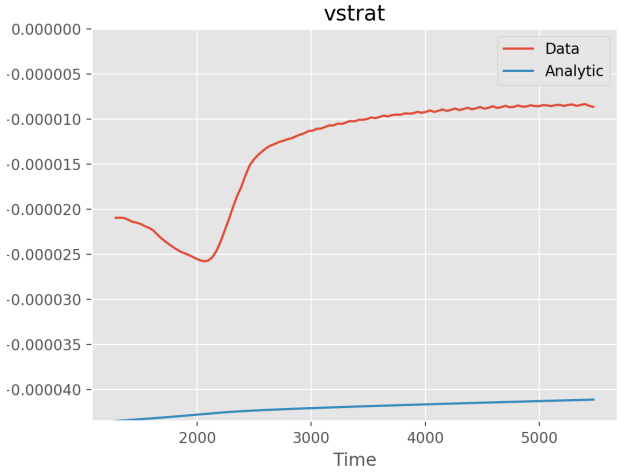

(b) Front velocity compared to analytical Eq. 11 prediction.

FIG. 9: Boussinesq data analysis plots.

Appendix A: Equation Implementations

We denote $x \in [0, L_x], z \in [0, L_z]$ the simulation domain and N_x, N_z the number of spectral modes in the respective dimensions.

1. Stratified Fluid

We introduce variable $T = P/\rho$. We then mandate ρ_0, T_0 background fields satisfy hydrostatic equilibrium $\vec{\nabla} T_0 + T_0 \vec{\nabla} \rho_0 + \vec{g} = 0$. Taking isothermal stratification, we find $T_0 = gH$. Making then substitution of variables $\Upsilon = \ln \rho - \ln \rho_0$ and $T_1 = T - T_0$ deviations from the background state, the exact fluid equations in the new variables are:

$$\vec{\nabla} \cdot \vec{u} = 0, \tag{A1a}$$

$$\frac{\partial \Upsilon}{\partial t} - \frac{u_z}{H} = 0, \tag{A1b}$$

$$\frac{\partial u_x}{\partial t} + \Big(\vec{u} \cdot \vec{\nabla}\Big) u_x + \frac{\partial T}{\partial x} + gH \frac{\partial \Upsilon}{\partial x} + T_1 \frac{\partial \Upsilon}{\partial x} = 0, \tag{A1c}$$

$$\frac{\partial u_z}{\partial t} + \Big(\vec{u} \cdot \vec{\nabla}\Big) u_z + \frac{\partial T}{\partial z} + gH \frac{\partial \Upsilon}{\partial z} + T_1 \frac{\partial \Upsilon}{\partial z} - \frac{T_1}{H} = 0. \tag{A1d}$$

These are implemented as:

$$\vec{\nabla} \cdot \vec{u} = 0, \tag{A2a}$$

$$\frac{\partial \Upsilon}{\partial t} - \frac{u_z}{H} - \nu \nabla^2 \Upsilon = -\Gamma(z) \Upsilon - \Big(\vec{u} \cdot \vec{\nabla}\Big) \Upsilon + \frac{F}{\rho_0(z)} e^{-\frac{(z-z_0)^2}{2\sigma^2}} \cos(k_x x - \omega t), \tag{A2b}$$

$$\frac{\partial u_x}{\partial t} + \frac{\partial T}{\partial x} + gH \frac{\partial \Upsilon}{\partial x} - \nu \nabla^2 u_x = -\Gamma(z) u_x - \Big(\vec{u} \cdot \vec{\nabla}\Big) u_x - T_1 \frac{\partial \Upsilon}{\partial x}, \tag{A2c}$$

$$\frac{\partial u_z}{\partial t} + \frac{\partial T}{\partial z} + gH \frac{\partial \Upsilon}{\partial z} - \frac{T_1}{H} - \nu \nabla^2 u_z = -\Gamma(z) u_z - \Big(\vec{u} \cdot \vec{\nabla}\Big) u_z - T_1 \frac{\partial \Upsilon}{\partial z}, \tag{A2d}$$

$$\Gamma(z) = 7.5 \left[2 + \tanh \frac{z - z_T}{(L_z - z_T)/2} + \tanh \frac{z_B - z}{z_B/2} \right], \tag{A2e}$$

where $z_B = 0.05 L_z, z_T = 0.95 L_z$ are the boundaries of the damping zones. A Navier-Stokes numerical viscosity ν is used to damp high wavenumbers and regularize the nonlinear cascade at near grid resolution: $\nu \sim 0.2 \frac{\omega}{|k_z|} \frac{L_z}{2\pi N_z}$ was found to be suitable for $N_z = 1024$, where k_z is the wavenumber of the excited linear mode.

2. Boussinesq Fluid

In the Boussinesq system, there is no need to transform to T, Υ variables as ρ_0 is constant. Including numerical terms and driving terms, our full equations are

$$\vec{\nabla} \cdot \vec{u}_1 = 0, \tag{A3a}$$

$$\frac{\partial \rho_1}{\partial t} - \frac{\rho_0 u_z}{H} - \nu \nabla^6 \rho_1 = -\Gamma(z) \rho_1 - \Big(\vec{u} \cdot \vec{\nabla}\Big) \rho_1 + F e^{-\frac{(z-z_0)^2}{2\sigma^2}} \cos(k_x x - \omega t), \tag{A3b}$$

$$\frac{\partial u_x}{\partial t} + \frac{\partial_x P}{\rho_0} - \nu \nabla^6 u_x = -\Gamma(z) u_x - \Big(\vec{u} \cdot \vec{\nabla}\Big) u_x, \tag{A3c}$$

$$\frac{\partial u_z}{\partial t} + \frac{\partial_z P}{\rho_0} + \frac{\rho_1 g}{\rho_0} - \nu \nabla^6 u_z = -\Gamma(z) u_z - \Big(\vec{u} \cdot \vec{\nabla}\Big) u_z. \tag{A3d}$$

$\Gamma(z)$ is as Eq. A2e. We use subgrid model ∇^6 (cite) to decrease the effect of viscosity on scales above the grid resolution.